

Daniel Portalez
Gautier Rollin
Pierre Leandri
Benjamin Elman
Patrick Mouly
Frédéric Jonca
Bernard Malavaud

Prospective comparison of T2w-MRI and dynamic-contrast-enhanced MRI, 3D-MR spectroscopic imaging or diffusion-weighted MRI in repeat TRUS-guided biopsies

Received: 24 February 2010
Revised: 28 April 2010
Accepted: 24 May 2010
Published online: 3 August 2010
© European Society of Radiology 2010

D. Portalez
Department of Radiology,
Clinique Pasteur, 45,
avenue de Lombez, 31300 Toulouse,
France

G. Rollin · P. Mouly · F. Jonca ·
B. Malavaud (✉)
Department of Urology,
Hôpital de Rangueil,
1, avenue Jean Poulhès, TSA 50032-31059
Toulouse Cedex 9, France
e-mail: malavaud.b@chu-toulouse.fr
Tel.: +33-561-323229
Fax: +33-561-323230

P. Leandri
Department of Urology,
Clinique Saint Jean, 20,
Route de Revel, 31400 Toulouse, France

B. Elman
Department of Urology,
Clinique Pasteur, 45,
avenue de Lombez, 31300 Toulouse,
France

Abstract *Objectives* To compare T2-weighted MRI and functional MRI techniques in guiding repeat prostate biopsies. *Methods* Sixty-eight patients with a history of negative biopsies, negative digital rectal examination and elevated PSA were imaged before repeat biopsies. Dichotomous criteria were used with visual validation of T2-weighted MRI, dynamic contrast-enhanced MRI and literature-derived cut-offs for 3D-spectroscopy MRI (choline-creatine-to-citrate ratio >0.86) and diffusion-weighted imaging ($ADC \times 10^3 \text{ mm}^2/\text{s} < 1.24$). For each segment and MRI technique, results were rendered as being suspicious/non-suspicious for malignancy. Sextant biopsies, transition zone biopsies and at least two additional biopsies of suspicious areas were taken. *Results* In the peripheral zones, 105/408 segments and in the transition zones 19/136 segments were suspicious according to at least one

MRI technique. A total of 28/68 (41.2%) patients were found to have cancer. Diffusion-weighted imaging exhibited the highest positive predictive value (0.52) compared with T2-weighted MRI (0.29), dynamic contrast-enhanced MRI (0.33) and 3D-spectroscopy MRI (0.25). Logistic regression showed the probability of cancer in a segment increasing 12-fold when T2-weighted and diffusion-weighted imaging MRI were both suspicious (63.4%) compared with both being non-suspicious (5.2%). *Conclusion* The proposed system of analysis and reporting could prove clinically relevant in the decision whether to repeat targeted biopsies.

Keywords Prostate cancer · Biopsies · T2w-MRI · DCE-MRI · DWI-MRI

Introduction

New cases of prostate cancer are expected to occur in more than 190,000 patients in the United States in 2009, where the disease is the second leading cause of cancer deaths in males [1].

Since its introduction, prostate-specific antigen (PSA) has generally been considered to be dichotomous and values greater than a fixed threshold have been considered valid indications for biopsies. This strategy was recently suggested in the European Randomised Screening for Prostate Cancer trial not only to increase cancer detection but also to reduce 10-year cancer-specific mortality

although at the expense of over-diagnosis and over-treatment [2]. Of note, such a reduction in cancer-specific mortality was not confirmed in the Prostate Lung Colorectal and Ovarian cancer screening trial [3], making the decision to promote prostate cancer screening an open issue.

Transrectal ultrasound (TRUS)-guided laterally directed 18G core biopsies of the peripheral zone are recommended to obtain material for examination [4]. When performing biopsy, one has to move the probe to mentally integrate the real-time 2D images into a 3D representation of the anatomical environment in order to regularly sample the prostate and maximise the probability of

detecting cancer [5]. Such mental reconstruction can explain limitations in diagnostic performance of randomised sextant biopsies, as first illustrated by Levine, who analysed the results of 137 men subjected to two consecutive sets of biopsies in a single office visit and showed that 30% of the cancers were detected exclusively in the second biopsy set [6]. This was then confirmed in the European Prostate Cancer Detection Study where, in 820/1,051 patients with negative first TRUS-guided biopsies, cancer was detected in 10% (83) on re-biopsy [7].

Therefore progress in MRI detection could lead to a paradigm shift in diagnosis from randomised sextant biopsies to directed biopsies of areas with features which raised the suspicion of tumour [8].

However, prostate MRI comprises distinct imaging techniques that have rarely been compared in prostate cancer detection. Classical T2-weighted MR imaging can depict cancer as a low-intensity area in the peripheral zone (PZ) albeit with low specificity. Dynamic contrast-enhanced MR imaging (DCE-MRI) and 3D-MR spectroscopic imaging (MRSI) improve prostate cancer detection, but substantial limitations remain such as chronic prostatitis, post-biopsy changes, glandular atrophy, prostatic intraepithelial neoplasia and cancer arising in the transition zone. Diffusion-weighted MRI (DWI) was recently proven to increase prostate cancer detection [9].

The present prospective study of 68 patients with normal digital rectal examination (DRE) and negative previous biopsies was therefore designed to assert the relevance of T2-weighted MRI alone or in combination with functional MRI techniques in guiding repeat transrectal ultrasound-guided biopsies.

Materials and methods

Patients

This prospective study was approved by the Institutional Review Board of our hospital, and written informed consent was obtained from all patients. From November 2007 to July 2008, 68 patients with a history of negative transrectal ultrasound-guided biopsies of the prostate were referred for MR imaging before repeat biopsies for negative DRE and elevated PSA. All patients had been sampled before MRI following the standards of the referring centres [mean number of cores taken 17.1 ± 10.1 , mean number of negative sets of biopsies 1.14 (range 1–4)]. The interval between the last set of biopsies and MR imaging ranged from 6 to 13 months (mean 8.3 ± 1.9 months).

Imaging methods

The study was carried out on a 1.5T MR imaging system (Achieva, Philips Medical Systems, Best, The Nether-

lands) using an integrated endorectal-pelvic coil (Philips Medical Systems, Best, The Netherlands). The coil was inserted in the lateral position and inflated with 50 mL of air; peristalsis was not suppressed. For DWI, a sensitivity encoding (SENSE) cardiac coil (five receiver coils) was preferred to an endorectal coil (single receiver coil) as it was shown to enhance the quality of diffusion-weighted echo planar imaging (EPI) by reducing blurring and off-resonance artefacts [10].

Patients were imaged in the supine position according to the manufacturer's recommendations as summarised in Table 1. Briefly, conventional thin transverse turbo spin-echo T2-weighted (T2-w MRI) anatomical images were first acquired. Diffusion-weighted imaging (DWI) with SENSE-EPI single-shot sequence was then performed before obtaining ADC (apparent diffusion coefficient) images with b values of 0 and 600 s/mm^2 in the same planes as T2-weighted sequences. For DWI, a sense factor of 2 was selected to minimise time of echo (TE) and associated susceptibility artefacts, so that a large field of view was necessary to avoid aliasing artefacts with SENSE.

3D-MR spectroscopy imaging with point-resolved 3D pre-selection volume (PRESS) was performed thereafter. Saturation and inversion recovery techniques were used to suppress water and fat respectively. Contamination from adjacent prostatic tissues was eliminated using outer volume saturation pulses. Six to 12 voxels per slice were symmetrically positioned in the medial, intermediate and lateral aspects of the prostate. Voxel analysis was performed using standard software.

Finally, dynamic-contrast-enhanced MRI was obtained by fat-saturated T1-weighted fast-field echo sequence (FFE). Following acquisition of T1 relaxation data, 14 consecutive dynamic sequences were acquired after an intravenous bolus injection of 20 ml of gadoterate meglumine (Dotarem, Guerbet, Roissy, France).

T2-w MRI, DCE-MRI, DWI and MRSI were successfully performed in all patients. The overall examination time ranged from 40 to 45 min, including coil placement and patient positioning.

MR image and MR spectroscopic image interpretation

All MRI analyses were performed by the same uro-radiologist (D.P., 10 years of experience in prostate MRI imaging) on an Extended WorkSpace workstation (Philips Healthcare, Best, The Netherlands). Interpretation started with assessment of the prostate morphology (T2-w MRI) before functional imaging. For each technique, results were reported as being positive or negative on the basis of diagnostic criteria established in three reference clinical series [9, 11, 12] and presented for eight prostate segments corresponding to the six standard peripheral zone segments and two left and right transition zone segments.

T2-w MRI Suspicious findings consisted of hypointense ovoid mass-like or nodular subcapsular foci of reduced

Table 1 Parameters used in the present series for prostate cancer MRI

	T2-weighted MRI (T2w-MRI)	Dynamic contrast enhancement MRI (DCE-MRI)	Diffusion weighted imaging (DWI)	3D Magnetic resonance spectroscopic imaging (3D-MRSI)
Coil and sequence	Endorectal coil; TR/TE 3,300/130 ms	Endorectal coil; fat-saturated T1-weighted FFE, 3D scan mode, TR/TE: 11 ms/4.6 ms	Sense-cardiac coil; TR/TE shortest possible/72 ms	Endorectal coil PRESS; TR/TE 1,500/120 ms
Slice parameters	Thickness 2.5 mm, gap 0.25 mm	Thickness 3 mm, gap 0 mm	Thickness 5 mm, SENSE sequence with P reduction 2.00	T2 preview transverse section: 3-4 slices, thickness 15 mm
FOV and matrix	FOV: 170×153 mm, TSE factor 20; voxel size 0.72×0.96 mm	FOV: 130×116 mm; flip angle 25°; voxel size 1.16×1.16 mm	FOV: 370×286 mm; flip angle 90°; voxel size 2.26×2.89 mm	FOV: 80×80 mm; voxel size 8.0×8.0×9.0 mm
Functional imaging		14 Consecutive post gadolinium dynamic sequences (same parameters); reconstruction voxel 0.51×0.51×5.0	Acquisition for diffusion-weighted ADC: b values 0 and 600 s/mm ² , obtained in the same planes as T2; reconstruction voxel 1.93×1.95×5.0	BASING pulse sequence (8 slices); acquisition voxel size 8.5×8.89×8.0; reconstruction voxel 8.5×8.5×8.5
Duration	1 min 45 s	13 s/sequence, total 3 min 36 s plus gadolinium injection	First acquisition 1 min 47 s; second acquisition for diffusion-weighted ADC 1 min 20 s	17 min 21 s

TR/TE Time of repetition (ms)/time of echo (ms), FOV field of view, ADC apparent diffusion coefficient, PRESS point-resolved spectroscopy, FFE fast field echo

signal intensity in the peripheral zone (Fig. 1a). For the transition zone, as described by Akin et al., homogeneous low T2 signal intensity with ill-defined margins and lack of capsule or invasion of the anterior fibro-muscular stroma were also considered significant [13].

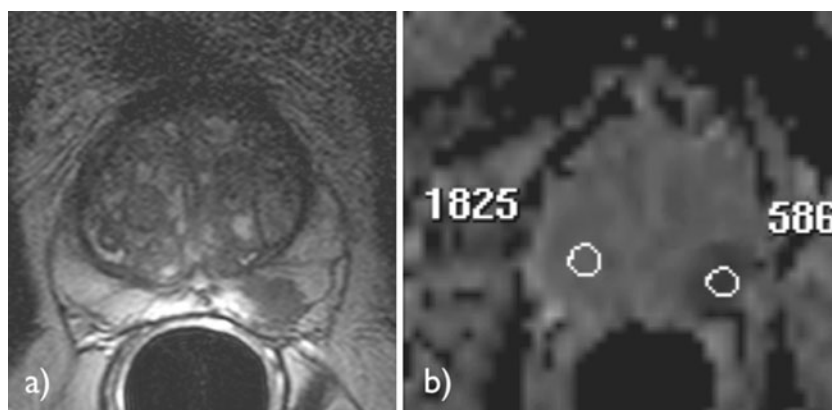
DWI ADC of predetermined ROI were drawn on all transverse sections, calculated and compared with the contralateral location (e.g. peripheral zone right apex was compared with the peripheral zone left apex) (Fig. 1b). If needed, complementary ROI were added to analyse areas that were suspicious according to T2-w MRI or DWI. Reinsberg et al. [9] reported that healthy tissues exhibited $ADC \times 10^{-3} \text{ mm}^2/\text{s}$ values of 1.51 ± 0.27 for the peripheral zone and 1.31 ± 0.20 for the transition zone so that lower values should be considered suspicious for prostate cancer. We therefore used the mean value minus SD (≤ 1.24 and ≤ 1.11 in the peripheral zone and the transition zone respectively) as the cut-off. Any lower values were considered suspicious in the present study.

MRSI All peripheral zone voxels were analysed (Fig. 2). Following the pivotal work by Jung [14], and in line with Fütterer et al. [11], a voxel was considered as definitely suspicious for malignant tissue (malignancy score 5) when the choline-creatine-to-citrate ratio was greater than 0.86. As reviewed by Westphalen et al., in the rare event of an uneven baseline, computer calculation of the choline-creatine-to-citrate ratio can be misleading [15], so all calculations were validated visually. For the transition zone, we used Zakian's criterion, where a voxel was considered positive when only choline was detected [16].

DCE-MRI Enhancement analysis was performed on an Extended Workspace workstation (Philips Healthcare, Best, The Netherlands). After subtraction of the fat-saturated T1-weighted FFE data acquired before gadoterate meglumine injection, grey-scale DCE-MRI images were visualised for all sections of the gland at the four first time points as it was shown that signal intensity enhancement is observed earlier in cancer tissue than in healthy tissue (Fig. 3). Among the ten parameters generated by the workstation, the four referred to in the DCE-MRI literature were taken into account. Automatic colour-coding of the parameters was used to draw attention to abnormal contrast-enhancement areas. Regions of interest were then drawn symmetrically within the peripheral and transition zones over either hypointense areas on T2-weighted images or on software colour-coded areas that represented enhanced contrast in comparison to the contralateral control area.

As illustrated in Fig. 3, the resulting data comprised maximum relative enhancement, wash-in rate, time-to-peak and wash-out information, which were fitted by the software to the time-signal intensity curves. As described by Engelbrecht et al., short time-to-peak, peak enhance-

Fig. 1 A 71-year-old man with prostate cancer in the left lobe. **a** Low signal intensity in the left part of the peripheral zone on an axial T2-weighted transverse MR image. **b** Diffusion-weighted image with an axial ADC map at the same axial section as defined on the T2-weighted image showing suspicious ADC value ($0.586 \times 10^{-3} \text{ mm}^2/\text{s}$) in the left lobe and healthy tissue ADC value ($1.825 \times 10^{-3} \text{ mm}^2/\text{s}$) in the right lobe



ment and wash-out within the experiment were considered evocative of prostate cancer in the peripheral zone [12]. In the transition zone where early wash-out is routinely observed in healthy tissue, suspicion was driven by the combination of shorter time-to-peak, higher peak enhancement and more rapid wash-out than observed in the rest of

the transition zone. Qualitative analysis of time-signal intensity curves was performed. As reviewed by Choi et al. for the peripheral zone [17], type 1 curves were considered suspicious for cancer and type 2 curves non-suspicious (Fig. 3c). Intermediate curves were also considered non-suspicious.

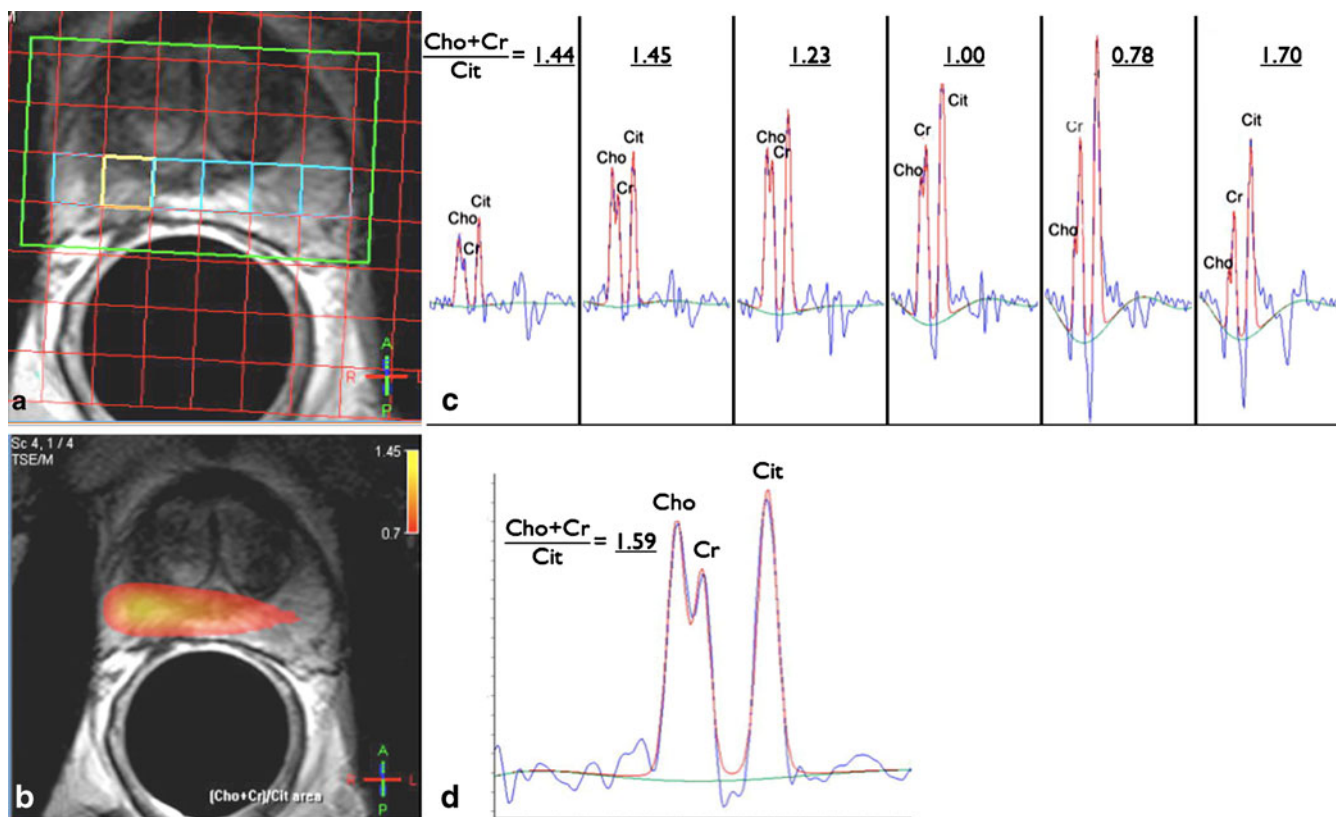


Fig. 2 A 59-year-old man with prostate cancer in the right lobe. **a** MR spectroscopic imaging grid superimposed on transverse T2-weighted MR image. The *green box* indicates the pre-selected volume for MRSI, the *blue boxes* indicate the voxels selected for analysis and the *yellow box* indicates the voxel selected for interpretation. An area of decreased intensity is observed in the right lobe on the T2-w MR image. **b** Choline + creatine/citrate (Ch+Cr/Ci) map showing higher values in the right lobe (*red*) and a

greater suspicious area in the right peripheral zone (*yellow*) than in the left lobe. **c** Corresponding spectra of the areas outlined on the *imaging grid* that are evocative of cancer in the right lobe (Ch+Cr/Ci=1.45) and suggestive of healthy tissue in the left lobe (Ch+Cr/Ci=0.70). **d** Suspicious spectrum in the yellow voxel of the right lobe corresponding to the low signal intensity on T2-w MRI. The *green line* represents the baseline, the *blue line* the acquired spectrum. The *red line* is generated by standard software

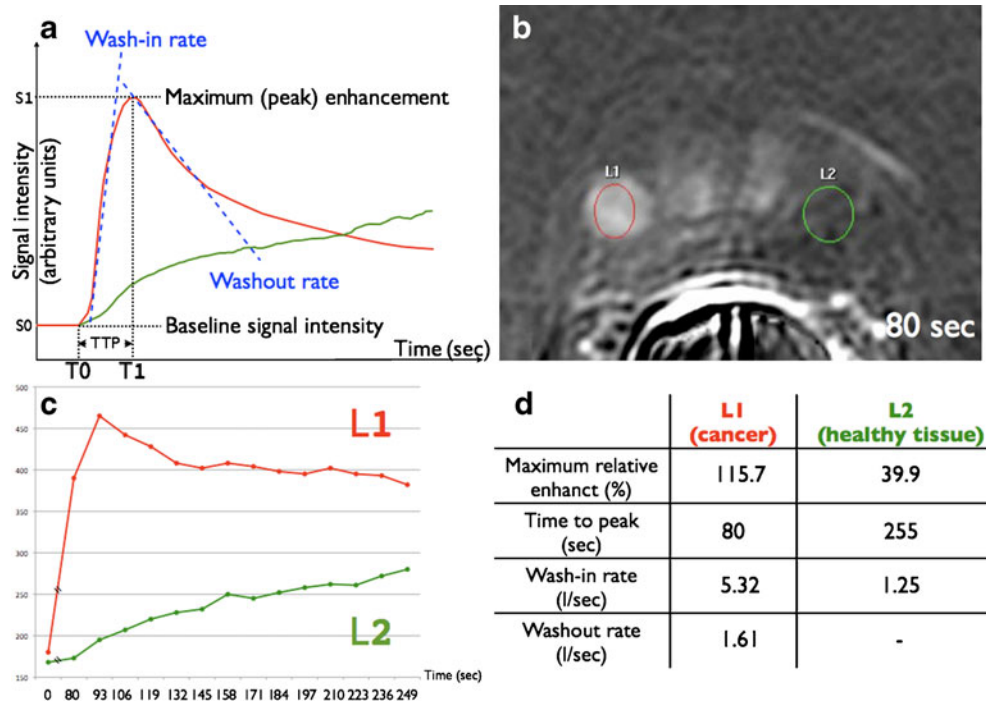


Fig. 3 Schematic presentation and representative case of DCE-MRI. **a** Time-signal intensity curves from dynamic contrast-enhanced MR imaging showing higher and faster enhancement and faster wash-out in cancer tissue (*L1*) than in healthy tissue (*L2*). *S*₀ represents baseline intensity in arbitrary units, *S*₁ signal intensity at absolute peak enhancement. The time-to-peak (*TTP*) is the period between the onset time (*T*₀) and peak enhancement (*T*₁). The wash-in rate represents the velocity of enhancement and is defined by $S_1 - S_0 / T_1 - T_0$. Maximum relative enhancement is defined as the difference between *S*₁ and *S*₀. The wash-out rate is defined as the velocity of enhancement loss. **b** A 64-year-old patient with prostate cancer in the

right lobe. DCE-MRI shows an increased signal in the peripheral zone of the right lobe. Circles are drawn symmetrically in the right (*L1*) and the left (*L2*) peripheral zones. An area of increased signal is included in the *right circle*. **c** Time-signal intensity curves for the two regions of interest showing shorter time-to-peak, higher wash-in rate, maximum relative enhancement and wash-out in *L1* (cancer) compared with *L2* where a steady increase in signal intensity is typical of healthy tissue. **d** Corresponding calculated parameters confirming shorter time-to-peak, higher wash-in rate, maximum relative enhancement and wash-out in *L1*

Biopsies

A systematic sextant pattern was first used with biopsies taken at the base, middle and apex of the right and left peripheral zones lateral to the parasagittal plane. Two transition zone biopsies were also taken. The number of biopsies per segment was adapted to the age of the patient and the volume of the prostate according to the Vienna nomogram [18]. Biopsies were performed by the referring physician (radiologist D.P., urologists: P.L., P.M., F.J., B.M.), during axial transverse imaging with an 18-gauge biopsy cut needle driven by a spring-loaded biopsy gun.

Additional biopsies were then targeted by the same operator towards areas with features which raised the suspicion of tumour (Fig. 4). For that purpose, suspicious segments, irrespective of the MRI technique used to detect them, were automatically transferred by the software onto T2w-MR images, which most resemble those routinely obtained by transrectal ultrasound. TRUS-guided biopsies

were then obtained adjusting for the change in obliquity between MRI techniques and TRUS. The total number of biopsies as well as biopsy results were recorded for each segment. The mean interval between MR imaging and biopsy was 11 days (range 2–22 days).

Statistical analysis

The elementary unit for analysis was the segment (6+2 segments plus suspicious areas if any) annotated with corresponding MRI results expressed in a dichotomous manner as suspicious or non-suspicious and the biopsy results. The crude probability of getting a positive biopsy was calculated as the ratio of positive biopsies to the total number of biopsies taken.

Contingency tables were created to illustrate the relationship between T2w-MRI /DWI/MRSI/DCE findings and biopsy results. Yates's corrected chi-squared test was used to evaluate the association between categorical

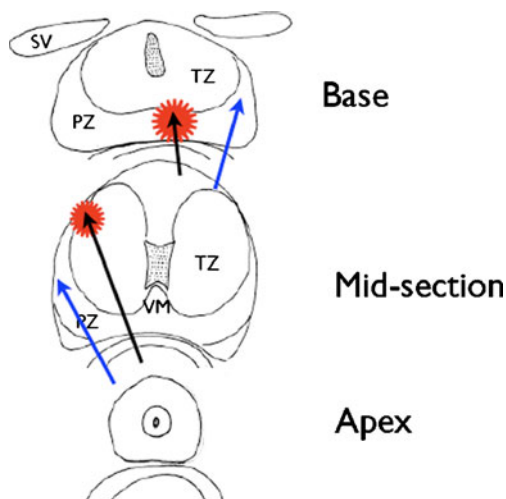


Fig. 4 Representation of the differences in obliquity and direction of sextant biopsies (blue arrow) and additional biopsies (black arrow) taken in MRI-suspicious areas (red stars)

variables and biopsy results. Statistical significance was set at $P < 0.05$. All reported P values are two-sided.

To evaluate the diagnostic performances of each MRI technique, sensitivity, specificity, accuracy, positive predictive value and negative predictive value were calculated. To assert the probability of obtaining positive repeat biopsies from the results of T2-w MRI and functional imaging, logistic regression modelling was conducted with the results of repeat biopsies as independent variables and T2-w MRI and functional technique results as dependent variables. The probability of a positive biopsy was then calculated by the probability function $\exp(x)/[1+\exp(x)]$ where x is the linear combination of T2-w MRI and functional MRI results (suspicious = 1, non-suspicious = 0) multiplied by their regression coefficients [19].

For a given combination of MRI results (e.g. segment positive for T2 and DCE but negative for DWI) the probability of getting a positive biopsy calculated from logistic regression was then compared with the crude probability as defined above.

Results

Sixty-eight consecutive patients were enrolled. Mean age was 62.4 years (range 49–76 years), and mean serum PSA level was 9.16 ng/ml (range 1.6–25 ng/ml). The mean number of repeat biopsies (18 gauge, 19 mm length each) was 18.1 (range 12–34) as the sum total of systematic biopsies (range 10–20) and of two additional biopsies of any suspicious areas (range 2–14).

Four hundred and eight segments in the PZ and 136 segments in the TZ were assessed, of which 105/408 in the PZ and 19/136 in the TZ were considered suspicious according to at least one MRI technique. Prostate cancer was found in 28/68 (41.2%) patients corresponding to forty-five segments (41PZ, 4 TZ).

In 62 segments suspicious areas were found to occur in locations not sampled by sextant biopsies—such as the anterior or medial aspects of the peripheral part of the segment (Fig. 4)—of which 20 (32%) were found to be positive. The other 25 positive segments were found in the routine eight spots. Foci of chronic prostatitis, glandular atrophy and high-grade prostatic intraepithelial neoplasia were found in 15, 6 and 12 patients respectively. As a whole, cancer was demonstrated in 41/408 (10.0%) segments in the peripheral zone and 4/136 (2.9%) in the transitional zone. In view of the limited number of cancers in the transition zone, further analysis focused on the peripheral zone only.

In the peripheral zone 68, 36, 48 and 31 segments were considered suspicious with T2w-MRI, DCE-MRI, MRSI and DWI respectively, of which 20 (29.4%), 12 (33.3%), 12 (25%) and 16 (51.6%) were found to be positive for cancer. Of note, T2w-MRI was unequivocal in six patients with prostate cancer, one of whom had non-suspicious findings with all four MRI techniques.

While all techniques exhibited excellent accuracy, negative predictive value and specificity in the peripheral zone, the choice of stringent cut-offs impacted sensitivity and positive predictive value with the highest sensitivity observed for T2w-MRI and the highest positive predictive value for DWI (Table 2).

As illustrated in Table 3, the probability of a segment being malignant was calculated from logistic regression

Table 2 Sensitivity, specificity, predictive values and accuracy of T2w-MRI, DCE-MRI, MRSI and DWI for per segment prediction of prostate cancer into 408 segments of peripheral zone

Peripheral zone	T2w-MRI	DCE-MRI	MRSI	DWI
Sensitivity	0.48	0.29	0.40	0.39
Specificity	0.87	0.93	0.89	0.96
Positive predictive value	0.29	0.33	0.25	0.52
Negative predictive value	0.94	0.92	0.94	0.93
Accuracy	0.83	0.86	0.85	0.90

T2w-MRI T2-weighted magnetic resonance imaging, DCE-MRI dynamic contrast-enhanced MRI, MRSI 3D-MR spectroscopic imaging, DWI diffusion-weighted MRI

Table 3 Per-segment prostate cancer probability of detection in 408 segments of peripheral zone from T2-w MRI results alone or combined with DCE-MRI, MRSI and DWI

Probability (%)		T2w-MRI	DCE-MRI		MRSI		DWI	
			Unsuspectious	Suspicious	Unsuspectious	Suspicious	Unsuspectious	Suspicious
T2-MRI	Unsuspectious	6.2	5.8	14.9	4.1	11.7	5.2	32.9
	Suspicious	29.4	22.4	44.7	17.8	39.7	16.2	63.4

T2w-MRI T2-weighted magnetic resonance imaging, *DCE-MRI* dynamic contrast-enhanced MRI, *MRSI* 3D-MR spectroscopic imaging, *DWI* diffusion-weighted MRI

modelling on the basis of the results of T2w-MRI and of any single functional technique:

$$\text{T2w - MRI + DCE - MRI probability} = \frac{e^{2.77-1.53 \cdot \text{T2} - 1.03 \cdot \text{DCE}}}{1 + e^{2.77-1.53 \cdot \text{T2} - 1.03 \cdot \text{DCE}}}$$

$$\text{T2w - MRI + MRSI probability} = \frac{e^{3.13-1.6 \cdot \text{T2} - 1.11 \cdot \text{MRSI}}}{1 + e^{3.13-1.6 \cdot \text{T2} - 1.11 \cdot \text{MRSI}}}$$

$$\text{T2w - MRI + DWI probability} = \frac{e^{2.9-1.26 \cdot \text{T2} - 2.19 \cdot \text{DWI}}}{1 + e^{2.9-1.26 \cdot \text{T2} - 2.19 \cdot \text{DWI}}}$$

Because 41 segments were found with cancer among the 408 segments sampled, a crude probability of 41/408 (10.0%) of a positive biopsy in any segment was calculated. The ratio of the probability of a given combination (e.g. T2w-MRI + DWI) to this figure was then used to illustrate the added value of the combination over undirected biopsies. This showed for instance a risk reduced by half when T2w-MRI and any of the three functional techniques were found to be non-suspicious as opposed to a six-fold increase when both T2w-MRI and DWI were suspicious in the same segment.

Discussion

We report a 41% detection rate in a series of 68 repeat-biopsy patients with non-suspicious digital rectal examination.

Although MRI criteria adapted from reports that addressed the limits of MRI imaging in that location were used for TZ interpretation [9, 13, 16], only a minority of TZ segments (19/136 TZ segments) were found suspicious, and cancer was detected in only four TZ segments in the present series. With a 3T MRI unit, Park recently reported that DWI achieved a high cancer detection rate in 43 patients with previous negative biopsies (17/43, 39.5%) [20]. Contrary to the present report, most of them (13/17, 76.4%) were located in the TZ. This might suggest a selection bias in the population subjected to MRI-guided biopsies or an advantage for cancer detection in the TZ with the 3T MRI unit.

As most cancers were detected in the peripheral zone (41/45) and very few in the transition zone (4/45), detection in the transition zone will not be further discussed in the present report. Similar to other series, all four MRI techniques exhibited excellent specificity (86.9–95.9%) and negative predictive value (92.1–94.1%), but were lacking in sensitivity and positive predictive value, except T2w-MRI whose sensitivity was good (48.8%) and DWI which showed an adequate positive predictive value (51.6%) suggesting that combining T2w-MRI with DWI might improve detection without impacting on specificity and negative predictive value. One classical limitation of positive and negative predictive values is that they are dependent on the prevalence of the disease in the study population. The proposed diagnostic criteria would therefore achieve different predictive values in other populations. The failure to reproduce in clinical series the results achieved in training sets is a classical limitation of any system of prognostication, notably when the results were obtained in research facilities distinct from routine clinical practice. This was recently highlighted in a prospective multi-institutional study of 110 patients due for radical prostatectomy who underwent presurgical T2w-MRI and MRSI using a standard 1.5T MRI system with a pelvic phased-array coil in combination with an endorectal coil [21]. As in the present study, the primary unit of analysis was the prostate sextant and the reference-standard finding was the presence or absence of cancer in the sextant on pathological analysis. The study showed that, contrary to single-institution preliminary reports [11, 22], MRSI did not add to conventional 1.5T endorectal imaging in terms of cancer localisation. In addition to the classical limitations of voxel size with the 1.5T system (0.60 cm³ in the present series) the discrepancy was in part attributed to the introduction of this recent technology to multiple centres with limited experience in MRSI interpretation [21]. This limitation was not entirely overcome by the proposed pre-defined five-point scale [14].

Indeed, a robust definition of suspicious and non-suspicious is needed to circumvent the classic trade-off between sensitivity and specificity when a discrete score of suspicion is used. This was well illustrated in the multi-institutional report mentioned above where ROC curves were produced in relation to the protocol's five-point score for T2w MRI and MRSI in biopsy-proven prostate cancer patients. Sensitivity and specificity varied over a wide range from 0.09 and 0.97 respectively for the highest suspicion score of 5 ("definitely malignant tissue") to 0.33 and 0.8 for a score of 4 ("probably malignant tissue") [21]. In order to produce unequivocal information for targeting repeat biopsies, the present series therefore

selected a dichotomous system of analysis (suspicious/non-suspicious).

In the challenging situation where previous biopsies were negative [23], clinically meaningful sensitivity and specificity were achieved (sensitivity 0.49, 0.29, 0.4 and 0.39, specificity 0.87, 0.93, 0.89, 0.96 for T2-w MRI, DCE-MRI, MRSI and DWI respectively), which compared well with the values observed by Weinreb et al. [21] in a more straightforward population of cancer-proven patients (score of 4: sensitivity 0.33, specificity 0.8).

The definition of the diagnostic criteria was based on seminal reports in the field of prostate cancer diagnosis with the use of thresholds for quantitative results such as those generated by MRSI and DWI. Because no clear consensus exists on optimal choline-creatine-to-citrate ratio cut-offs, we resorted to a ratio of 0.86 corresponding to the highest score (score 5 “definitely malignant tissue”) of the five-point scale proposed by Jung et al. [14] and validated by Fütterer et al. [11] in prostatectomy patients and Prando et al. [22] in patients with previous negative biopsies.

Because these reports were produced in the research setting with MRI units different from ours, the derived criteria used in the present series—although they proved to yield adequate results—will require further validation and may not represent the ultimate answer to a complex situation.

For DWI we used single-shot spin-echo echo-planar imaging with a SENSE cardiac coil with five receiver coils which, compared with the single-receiver endorectal coil, has the advantage of improving echo-planar imaging by reducing artefacts and enhancing spatial resolution [10]. Limiting factors include the overlap between ADC values of healthy and cancerous tissues [9], inter-individual variability, and intra-test variability in the same patient [24]. Technical factors, such as b values and the selection of the ROI, also play a role. Various b values have therefore been proposed as high values are preferred to reduce the signal contribution from capillary perfusion while low diffusion weighting attenuates the signal from fast-moving water molecules [25, 26]. As recently reviewed by Turkbey et al. [27], the use of higher b values (1,000, 2,000 s/mm²) improves lesion detection although it is associated with significant overlap between the signals of malignant and normal tissues. In a head-to-head comparison, Kitajima showed that selecting higher b values (2,000 vs. 1,000) was of little diagnostic advantage as it significantly altered (−21.6%) the signal-to-noise ratio [28] with no benefits in terms of contrast-to-noise ratio (−17.3%). The b value selection can therefore influence the distinction between malignant and normal tissue. Clinical reports were based either on a single b value ranging from 600 [29, 30] to 1,000 [24, 31] or on multiple b values (300, 500, 800) [9]. In line with the preliminary reports available at the initiation of this study, an intermediate b value of 600 and a monoexponential diffusion model were used in the present series [9, 29]. More recently, the inclusion of non-zero low b values and biexponential diffusion modelling [32] were proposed to improve the representation of fast tissue perfusion and to avoid the artefacts of pseudoperfusion [33, 34].

Generating normalised ADC by comparing ADC in the lesion and ADC in the contralateral location used as a reference has also been proposed [24], but this was not performed in the present series where a cut-off of <1.24, from Reinsberg, was used in the peripheral zone.

Dynamic contrast-enhancement analysis was based on the visual system proposed by Engelbrecht et al. [12]. Note that we were unable to obtain the reported seven sections in 2 s with the machine used here, for which the shortest time possible for a section was 13 s. Because little is known about the time-enhancement curves of prostate cancer and normal surrounding tissues [35], the influence, if any, on cancer detection remains to be determined. Very fast sequences (2 s), as proposed by the Nijmegen group, have the potential to highlight cancer lesions and to calculate micro-vascular permeability and maximum tissue gadolinium concentration through multi-compartmental analysis. This is achieved at the cost of low spatial resolution, thus to locate suspicious areas within the gland, DCE images must be superimposed on T2-weighted images using specific software [11]. Conversely, longer sequences (30 s) have optimal spatial resolution, but the early phase of enhancement cannot be studied and the number of acquisitions possible within the temporal imaging window where cancer enhancement is higher than that observed in healthy tissue is too small to permit compartmental analysis [35]. In a recent report, this group confirmed that visual criteria achieved an excellent compromise between sensitivity (0.52) and specificity (0.83) [36].

In order to visualise the early phase of cancer enhancement and retain spatial resolution (Fig. 3), we resorted to the shortest possible time with our MRI unit (13 s), which proved to yield adequate specificity (0.93) but suboptimal sensitivity (0.29). Qualitative detection of abnormalities in contrast enhancement spurred quantitative comparative analysis. When type 1 curves [17] were confirmed, the ROIs were labelled as being suspicious. Such two-step interpretation therefore amounted to semi-quantitative analysis that was shown to be better suited to the clinical setting than purely quantitative analysis [37].

However, fixed thresholds for quantitative parameters such as TTP, MRE, wash-in and wash-out rates would help to facilitate the learning curve and to avoid the classic pitfall of symmetrical cancer, where it is not possible to use contralateral healthy tissue as a reference [12]. However desirable, this objective is hard to achieve in view of individual variability and differences related to MRI units, techniques and even contrast agents. Adding to the confusion, some parameters such as time-to-peak that have strong intuitive meaning exhibit wide ranging values depending on the technique and the MRI unit. For instance, with the Magnetom Vision MRI unit (Siemens Medical Systems) and time resolution of 2.03 s, the Nijmegen group observed short (6–7 s) and comparable values in cancerous and healthy tissues [12], while with a unit similar to ours, Preziosi et al. [38] reported a 250 s mean for healthy tissue, which was significantly reduced in cancer (103 s).

As a whole, the current DCE semi-quantitative analysis exhibited some limitations but represented the best compromise available in the present clinical context.

This study produced the predictive values of four MRI techniques. It should be acknowledged that MRI analysis was conducted according to the current standard of interpretation in clinical care, i.e. when one technique was found to be suspicious in a given segment, special attention was paid to this segment with the three other MRI techniques, as befits the classic definition of a verification bias. This system of interpretation does not therefore permit the diagnostic values of the reported MRI techniques to be evaluated in a fully independent manner, which might constitute a limitation of the present study.

In the present series, we estimated the risk of getting a positive biopsy in a given segment, which, depending on imaging results, varied 15-fold from 4.1% (non-suspicious T2-w MRI and MRSI) to 63.4% (suspicious T2w-MRI and DWI). In practical terms, when referring to a crude proportion of positive biopsies of 10%, this amounted to a two-fold reduction in risk when both T2-w MRI and MRSI, DWI or DCE-MRI were non-suspicious to a six-fold increase in risk when both T2-w MRI and DWI were

suspicious. Probability diagrams, as proposed in Table 3, might prove of practical value in the shared decision to repeat biopsies in a given patient.

Conclusion

The present prospective head-to-head comparison of T2-w MRI and functional MRI techniques in the detection of prostate cancer showed comparable results in terms of sensitivity, specificity and negative predictive value for all techniques while there was a clear advantage for DWI in positive predictive value.

The proposed system has the advantage of using robust dichotomous criteria with visual validation of T2-w MRI, DCE and literature-derived cut-offs for MRSI and DWI. Based on a series of 68 patients with negative DRE and negative previous biopsies, the probability of a positive biopsy in a given segment was derived from imaging, showing for instance a 12-fold increase in risk when T2-w MRI and DWI were both suspicious (63.4% compared with 5.2% for non-suspicious). This system could prove clinically relevant in the decision whether or not to repeat targeted biopsies.

References

- Jemal A, Siegel R, Ward E, Hao Y, Xu J, Thun MJ (2009) Cancer statistics, 2009. *CA Cancer J Clin* 59:225–249
- Schroder FH, Hugosson J, Roobol MJ et al (2009) Screening and prostate-cancer mortality in a randomized European study. *N Engl J Med* 360:1320–1328
- Andriole GL, Crawford ED, Grubb RL 3rd et al (2009) Mortality results from a randomized prostate-cancer screening trial. *N Engl J Med* 360:1310–1319
- Heidenreich A, Aus G, Bolla M et al (2008) EAU guidelines on prostate cancer. *Eur Urol* 53:68–80
- Scalaverano S, Chevreau G, Vadcard L, Mozer P, Troccaz J (2009) BiopSym: a simulator for enhanced learning of ultrasound-guided prostate biopsy. *Stud Health Technol Inform* 142:301–306
- Levine MA, Ittman M, Melamed J, Lepor H (1998) Two consecutive sets of transrectal ultrasound guided sextant biopsies of the prostate for the detection of prostate cancer. *J Urol* 159:471–475, discussion 475–476
- Djavan B, Waldert M, Zlotta A et al (2001) Safety and morbidity of first and repeat transrectal ultrasound guided prostate needle biopsies: results of a prospective European prostate cancer detection study. *J Urol* 166:856–860
- Hricak H, Choyke PL, Eberhardt SC, Leibel SA, Scardino PT (2007) Imaging prostate cancer: a multidisciplinary perspective. *Radiology* 243:28–53
- Reinsberg SA, Payne GS, Riches SF et al (2007) Combined use of diffusion-weighted MRI and 1H MR spectroscopy to increase accuracy in prostate cancer detection. *AJR Am J Roentgenol* 188:91–98
- Bammer R, Auer M, Keeling SL et al (2002) Diffusion tensor imaging using single-shot SENSE-EPI. *Magn Reson Med* 48:128–136
- Futterer JJ, Heijmink SW, Scheenen TW et al (2006) Prostate cancer localization with dynamic contrast-enhanced MR imaging and proton MR spectroscopic imaging. *Radiology* 241:449–458
- Engelbrecht MR, Huisman HJ, Laheij RJ et al (2003) Discrimination of prostate cancer from normal peripheral zone and central gland tissue by using dynamic contrast-enhanced MR imaging. *Radiology* 229:248–254
- Akin O, Sala E, Moskowitz CS et al (2006) Transition zone prostate cancers: features, detection, localization, and staging at endorectal MR imaging. *Radiology* 239:784–792
- Jung JA, Coakley FV, Vigneron DB et al (2004) Prostate depiction at endorectal MR spectroscopic imaging: investigation of a standardized evaluation system. *Radiology* 233:701–708
- Westphalen AC, Coakley FV, Qayyum A et al (2008) Peripheral zone prostate cancer: accuracy of different interpretative approaches with MR and MR spectroscopic imaging. *Radiology* 246:177–184
- Zakian KL, Eberhardt S, Hricak H et al (2003) Transition zone prostate cancer: metabolic characteristics at 1H MR spectroscopic imaging—initial results. *Radiology* 229:241–247
- Choi YJ, Kim JK, Kim N, Kim KW, Choi EK, Cho KS (2007) Functional MR imaging of prostate cancer. *Radiographics* 27:63–75, discussion 75–77
- Remzi M, Fong YK, Dobrovits M et al (2005) The Vienna nomogram: validation of a novel biopsy strategy defining the optimal number of cores based on patient age and total prostate volume. *J Urol* 174:1256–1260, discussion 1260–1261; author reply 1261
- Vollmer RT (1996) Multivariate statistical analysis for pathologist. Part I, the logistic model. *Am J Clin Pathol* 105:115–126
- Park BK, Lee HM, Kim CK, Choi HY, Park JW (2008) Lesion localization in patients with a previous negative transrectal ultrasound biopsy and persistently elevated prostate specific antigen level using diffusion-weighted imaging at three Tesla before rebiopsy. *Invest Radiol* 43:789–793
- Weinreb JC, Blume JD, Coakley FV et al (2009) Prostate cancer: sextant localization at MR imaging and MR spectroscopic imaging before prostatectomy—results of ACRIN prospective multi-institutional clinicopathologic study. *Radiology* 251:122–133

22. Prando A, Kurhanewicz J, Borges AP, Oliveira EM Jr, Figueiredo E (2005) Prostatic biopsy directed with endorectal MR spectroscopic imaging findings in patients with elevated prostate specific antigen levels and prior negative biopsy findings: early experience. *Radiology* 236:903–910
23. Kelloff GJ, Choyke P, Coffey DS (2009) Challenges in clinical prostate cancer: role of imaging. *AJR Am J Roentgenol* 192:1455–1470
24. Lim HK, Kim JK, Kim KA, Cho KS (2009) Prostate cancer: apparent diffusion coefficient map with T2-weighted images for detection—a multireader study. *Radiology* 250:145–151
25. Koh DM, Collins DJ (2007) Diffusion-weighted MRI in the body: applications and challenges in oncology. *AJR Am J Roentgenol* 188:1622–1635
26. Le Bihan D, Breton E, Lallemand D, Aubin ML, Vignaud J, Laval-Jeantet M (1988) Separation of diffusion and perfusion in intravoxel incoherent motion MR imaging. *Radiology* 168:497–505
27. Turkbey B, Albert PS, Kurdziel K, Choyke PL (2009) Imaging localized prostate cancer: current approaches and new developments. *AJR Am J Roentgenol* 192:1471–1480
28. Kitajima K, Kaji Y, Kuroda K, Sugimura K (2008) High b-value diffusion-weighted imaging in normal and malignant peripheral zone tissue of the prostate: effect of signal-to-noise ratio. *Magn Reson Med* 7:93–99
29. Haider MA, van der Kwast TH, Tanguay J et al (2007) Combined T2-weighted and diffusion-weighted MRI for localization of prostate cancer. *AJR Am J Roentgenol* 189:323–328
30. Langer DL, van der Kwast TH, Evans AJ, Trachtenberg J, Wilson BC, Haider MA (2009) Prostate cancer detection with multi-parametric MRI: logistic regression analysis of quantitative T2, diffusion-weighted imaging, and dynamic contrast-enhanced MRI. *J Magn Reson Imaging* 30:327–334
31. Mazaheri Y, Shukla-Dave A, Hricak H et al (2008) Prostate cancer: identification with combined diffusion-weighted MR imaging and 3D 1H MR spectroscopic imaging—correlation with pathologic findings. *Radiology* 246:480–488
32. Mulkern RV, Barnes AS, Haker SJ et al (2006) Biexponential characterization of prostate tissue water diffusion decay curves over an extended b-factor range. *Magn Reson Imaging* 24:563–568
33. Riches SF, Hawtin K, Charles-Edwards EM, de Souza NM (2009) Diffusion-weighted imaging of the prostate and rectal wall: comparison of biexponential and monoexponential modelled diffusion and associated perfusion coefficients. *NMR Biomed* 22:318–325
34. Shinmoto H, Oshio K, Tanimoto A et al (2009) Biexponential apparent diffusion coefficients in prostate cancer. *Magn Reson Imaging* 27:355–359
35. Rouviere O, Raudrant A, Ecochard R et al (2003) Characterization of time-enhancement curves of benign and malignant prostate tissue at dynamic MR imaging. *Eur Radiol* 13:931–942
36. Cheikh AB, Girouin N, Colombel M et al (2009) Evaluation of T2-weighted and dynamic contrast-enhanced MRI in localizing prostate cancer before repeat biopsy. *Eur Radiol* 19:770–778
37. van Dorsten FA, van der Graaf M, Engelbrecht MR et al (2004) Combined quantitative dynamic contrast-enhanced MR imaging and (1)H MR spectroscopic imaging of human prostate cancer. *J Magn Reson Imaging* 20:279–287
38. Preziosi P, Orlacchio A, Di Giambattista G et al (2003) Enhancement patterns of prostate cancer in dynamic MRI. *Eur Radiol* 13:925–930